

# Journal of Materials Chemistry B

Accepted Manuscript



This is an *Accepted Manuscript*, which has been through the Royal Society of Chemistry peer review process and has been accepted for publication.

*Accepted Manuscripts* are published online shortly after acceptance, before technical editing, formatting and proof reading. Using this free service, authors can make their results available to the community, in citable form, before we publish the edited article. We will replace this *Accepted Manuscript* with the edited and formatted *Advance Article* as soon as it is available.

You can find more information about *Accepted Manuscripts* in the [Information for Authors](#).

Please note that technical editing may introduce minor changes to the text and/or graphics, which may alter content. The journal's standard [Terms & Conditions](#) and the [Ethical guidelines](#) still apply. In no event shall the Royal Society of Chemistry be held responsible for any errors or omissions in this *Accepted Manuscript* or any consequences arising from the use of any information it contains.

Cite this: DOI: 10.1039/c0xx00000x

PAPER

www.rsc.org/xxxxxx

## Ginsenoside nanoparticle: A new green drug delivery system

Lin Dai,<sup>a,b</sup> Kefeng Liu,<sup>a</sup> Chuanling Si,<sup>b</sup> Luying Wang,<sup>a</sup> Jing Liu,<sup>a</sup> Jing He,<sup>a</sup> Jiandu Lei<sup>\*a</sup>

Received (in XXX, XXX) Xth XXXXXXXXX 20XX, Accepted Xth XXXXXXXXX 20XX

DOI: 10.1039/b000000x

A large amount of chemosynthetic nano-drug carriers has to be used to administer a needed dose of a drug. However, high doses of these excipients may cause the emergence of toxic potential to the patients. Green chemistry aims to develop green nanoparticles loaded with drugs to reduce the use of toxic and harmful ingredients in the production process and provide the lower-dose prescribing for medical treatments. The use of non-toxic materials in pharmaceutical formulations could minimize the adverse effects of pharmaceutical residues entering the body and environment. Ginsenoside is a main bioactive constituent of herb Panax ginseng. Here, we firstly find that the ginsenoside Rb1 can self-assemble with anticancer drugs to form stable nanoparticles, which have greater anticancer effects *in vitro* and *in vivo* than the free drugs. The obtained nanoparticles possessed appropriate size (~100 nm), better tumor selectivity, high drug loading capacity (~35 wt% betulinic acid, ~32 wt% dihydroartemisinin, and ~21 wt% hydroxycamptothecin), and higher blood circulation half-time. Furthermore, the antitumor effect of the nanoparticles in a mouse tumor xenograft model exhibited much better tumor inhibition efficacy and fewer side effects than that of free drugs, strongly supporting their application as a novel efficient nanocarrier for anticancer therapy. Moreover, the ginsenoside nanoparticle with simple, green preparation method and easy large-scale production is promising for the delivery of various indissolvable drugs.

### 1. Introduction

When designing drug carriers, the drug-to-carrier ratio is an important consideration, because the carrier is still just an excipient for drug delivery and only the drug is the therapeutically relevant compound. Moreover, the use of high quantities of carriers can result in toxicity as a consequence of poor metabolism and elimination of the carriers.<sup>1</sup> Green chemistry aims to reduce or exclude the use or production of hazardous substances in the design, manufacture and application of chemical products.<sup>2</sup> Safety improvement is an important factor of green chemistry and green preparation,<sup>3</sup> and the production of pharmaceutical formulations can be manipulated by the application of non-toxic materials.<sup>4-7</sup>

Ginsenoside, the main bioactive constituent of a famous herb Panax ginseng, including (20S)-protopanaxadiol (Ppd) type based on their aglycone moieties, have been proven to be effective for prevention and treatment of cardiovascular and cerebrovascular disease. Ginsenoside Rb1 (Rb1) is the major Ppd type ginsenoside without toxicity. They exhibited many bioactivities including anticancer,<sup>8</sup> antioxidative,<sup>9, 10</sup> anti-inflammatory,<sup>11, 12</sup> inhibition of the vascular neointimal hyperplasia,<sup>13</sup> inducing angiogenesis,<sup>14</sup> and vasodilating action through the activation of nitric oxide in endothelial cells. Traditional Chinese medicine asserts that Panax quinquefolius promotes yin in the body.<sup>15, 16</sup>

The solubility of ginsenosides depends on the number of sugar

units in the structure. Ginsenosides have both hydrophobic triterpenes or steroid aglycones and hydrophilic sugar side chain(s) in their structures.<sup>17</sup> For an aglycone, sugar moieties that probably facilitate the dissolution of ginsenosides in water are absent, and therefore the solubility of an aglycone is lower than its corresponding glycoside. It was reported that many anticancer natural compounds have low aqueous solubility, such as betulinic acid (BA), dihydroartemisinin (DHA) and hydroxycamptothecin (HCPT), while the aqueous solubility of Rb1 were usually 100 folds higher.<sup>18</sup> Abundant studies have been done on the solubilization effect of saponin. They have been used as adjuvants to enhance the solubility or absorption of pharmacologically active substances or drugs in pharmaceutical preparations.<sup>19-22</sup> Increasing consumer demand for natural products has led to more attention on saponins, the “green natural additives”.

Nanoprecipitation is one of the common techniques through which we can increase the solubility of ginsenosides.<sup>19, 23</sup> An interesting phenomenon associated with dissolution of ginsenosides is self-assembled, which can increase their aqueous solubility by many folds. A typical nanoparticle in aqueous solution forms an aggregate with the hydrophilic “head” regions in contact with surrounding solvent, sequestering the hydrophobic single-tail regions in the nanoparticle center. When nanoparticle is formed, the water solubility of the test substance increases if we can locate these hydrophobic substances within the hydrophobic domain of the nanoparticles.<sup>24</sup> Moreover, tumors

have a special metabolism. Among the many differences with non-transformed tissues, perhaps the most relevant is that they rely on glucose as a source of energy and carbon. Tumors seek glucose so avidly, for this reason, glucose analogs could be used for targeted drug delivery in pharmaceutical applications.<sup>25</sup> Certain sugar modifications have been associated with reduced affinity for P-glycoprotein pumps and maintenance of cytotoxic activity. As described above, in the structure of ginsenosides, there is usually a lipophilic triterpene or steroidal aglycone attached to sugar side chain(s). We were inspired to design an improved delivery system in which the carrier would display therapeutic effects. This was achieved by utilizing the binding property of Rb1 with natural anticancer drugs such as BA, DHA, and HCPT. In the aqueous phase, the hydrophobic cores of polymeric nanoparticles are surrounded by hydrophilic outer shells. Thus, the inner core can serve as a nano-container for hydrophobic anticancer drugs. When injected into mice, the drug-loaded nanoparticle demonstrates better tumor selectivity and growth reduction, as well as longer blood half-life, than free drug.

## 2. Experimental Details

### 2.1. Reagents and materials

Ginsenoside Rb1 (Rb1), BA, DHA and HCPT were obtained from Chengdu Preferred Biotechnology Co., Ltd (Sichuan, China). All other reagents were purchased from Sigma Aldrich.

Fetal bovine serum (FBS) was from HyClone. Penicillin and streptomycin, Gibco Dulbecco's Modified Eagle's Medium (DMEM), Gibco Dulbecco's Phosphate-Buffered Saline (DPBS) were all bought from Invitrogen. Cell-Counting Kit-8 (CCK-8) kit was supplied by the Dojindo Laboratories. Murine Lewis lung carcinoma (LLC) cells and human lung cancer cells (A549) were obtained from the Peking University Health Science Center (Beijing, China) and were cultured in the listed medium: LLC by DMEM with 10% FBS, 1% streptomycin-penicillin and A549 by RPMI 1640 with 10% FBS, 1% streptomycin-penicillin. All cell lines were maintained in an incubator supplied with 5% CO<sub>2</sub>/95% air humidified atmosphere at 37 °C.

### 2.2. Animals and ethics

Female C57BL/6 mice, 6-7 weeks age, were purchased from Beijing HFK BIOSCIENCE CO., LTD. All the animal experiments were consistent with the guidelines set by the National Institutes of Health (NIH Publication No. 85-23, revised 1985) and were approved by the Experimental Animal Ethics Committee, Beijing.

### 2.3. Preparation of Rb1/drug nanoparticles (NPs)

Nanoparticles were prepared by a precipitation method according to previously reports.<sup>26</sup> BA was dissolved in DMSO (0.2 mL) at a concentration of 20 mg/mL, followed by injection into the water solution (1.8 mL) containing 3.5 mg/mL of ginsenoside Rb1 under magnetic stirring. Vortex for 10 min. The resulting Rb1/BA NPs solutions were transferred to a MWCO 1000 cartridge, and dialyzed against normal saline (50 mL) for 6 h with two exchanges of dialysate. The size of the particles was determined by dynamic light scattering with a particle analyzer (Zetasizer Nano-ZS, Malvern Instruments Ltd., Malvern, UK). Rb1/DHA NPs and Rb1/HCPT NPs were similarly prepared to that for Rb1/BA NPs.

### 2.4. Characterization of nanoparticles

Rb1/BA NPs, Rb1/DHA NPs and Rb1/HCPT NPs were diluted 100 × in deionized water, and a 2 μL aliquot of solution was pipetted onto the surface of Formvar coated copper TEM grids (Ted Pella, Redding, CA) and allowed to air-dry. Analysis was performed on a JEM-100CXa TEM at an acceleration voltage of 100 kV. The hydrodynamic size and zeta potential of nanoparticles were measured by a Nano-ZS Zeta Sizer (Malvern Instruments Ltd., Malvern, UK).

### 2.5. Determination of drug loading and *in vitro* drug release

The releases of drugs from the nanoparticles were analyzed by a dialysis method. Rb1/BA NPs, Rb1/DHA NPs and Rb1/HCPT NPs PBS solution (1 mg/mL, 5 mL) at pH 7.4 or 4.5 was loaded into a dialysis bag (MWCO 1000). Then the dialysis bag was immersed in 200 mL of PBS buffer (pH 7.4), citrate-phosphate buffer (pH 4.5) at 37 °C with gentle agitation. PBS medium (2 mL) was withdrawn at timed intervals and the BA, DHA, and HCPT concentration in the medium was determined by HPLC method (BA: 210 nm, 85:15 mixture (v/v) of acetonitrile-water as a mobile phase, flow rate at 1.0 mL/min. DHA: 210 nm, 60% of acetonitrile in 0.05% TFA at a flow rate of 1.0 mL/min. HCPT: 254 nm, 30:70 mixture (v/v) of acetonitrile-water as a mobile phase, flow rate of 1.0 mL/min) using a reverse phase column (VYDAC 214TP54, C18, 300A, 5 μm, 4.6×250 mm).<sup>27</sup> The amount released was then calculated. Each stability profile represents the average of three independent runs with the same sampling schedules. The standard deviation of each point is typically 2% or less. Drug loading capacity (DLC) were calculated according to the following equation: DLC (%) = (weight of loaded drug/weight of nanoparticles) × 100%. Esterase (30 units) was added into the dialysis bag when the BA release in the presence of esterase was studied.

### 2.6. Hemolysis assay

The hemolytic activity of polymer solutions was described as follows.<sup>28, 29</sup> Ten milliliters of fresh blood samples were collected from mice, and then added with EDTA-Na<sub>2</sub> immediately to prevent coagulation. The red blood cells (RBCs) were collected by centrifugation at 1500 rpm for 10 min at 4 °C. After washing in ice-cold DPBS until the supernatant was clear, erythrocytes were diluted to 5×10<sup>8</sup> cells/mL in ice-cold DPBS. 1mL (1 mg/mL and 0.1 mg/mL) Rb1 NPs, Rb1/BA NPs, Rb1/DHA NPs, Rb1/HCPT NPs, or PEI<sub>25K</sub> solution was mixed with 1 mL erythrocyte suspension. 1% Triton X-100 in DPBS and DPBS were used as positive control (100% lysis) and negative control (0% lysis), respectively. Samples were incubated under constant shaking for 1 h at 37 °C. After centrifugation at 1500 rpm for 10 min at 4 °C, supernatant was analyzed for hemoglobin release at 541 nm using an infinite M200 microplate spectrophotometer (Tecan, Switzerland). Hemoglobin release was calculated as (OD<sub>sample</sub> - OD<sub>negative control</sub>) / (OD<sub>positive control</sub> - OD<sub>negative control</sub>) × 100%. Hemolysis was determined from three independent experiments.

### 2.7. *In vitro* cell cytotoxicity

CCK-8 assay was used to evaluation the cell viability of different samples.<sup>30</sup> Briefly, two types of lung cancer cells LLC and A549 cells were respectively seeded at a density of 3×10<sup>3</sup> and 4×10<sup>3</sup>

cells/well in 180  $\mu\text{L}$  culture medium and incubated for 24 h. Then, the cells were treated with various samples (BA, DHA, HCPT, Rb1 NPs, Rb1/BA NPs, Rb1/DHA NPs and Rb1/HCPT NPs) at 37  $^{\circ}\text{C}$  in a humidified incubator with 5%  $\text{CO}_2$  for 72 h, where the samples of the BA, DHA, and HCPT were dissolved in dimethylsulfoxide (Merck, Darmstadt, Germany) and diluted into tissue culture medium before assay. Rb1/BA NPs, Rb1/DHA NPs and Rb1/HCPT NPs dose equal to free drugs, respectively. It is note that the Rb1+BA (or Rb1+DHA, Rb1+HCPT) stated in this article refer to adding Rb1 and BA (or DHA, HCPT) directly (the concentration of Rb1 10  $\mu\text{g}/\text{mL}$ , for BA was equal to native BA. 20  $\mu\text{L}$  of CCK-8 solution was added to each well and incubated for 1 h at 37  $^{\circ}\text{C}$ . Percent of cell viability can be calculated by measured the absence of the samples at 450 nm. The  $\text{IC}_{50}$  was got as sample concentrations which inhibited growth of 50% of cells relative to non-treated cells according to Unger et al.<sup>31</sup>  $\text{IC}_{50}$  was calculated using the Boltzmann sigmoidal function from Origin<sup>®</sup> 8.6 (OriginLab, Northampton, USA). Data are representative of three independent experiments.

## 2.8. Cellular uptake study

Cellular uptake and distribution of HCPT from nanoparticles were observed by confocal laser scanning microscopy (CLSM). After LLC cells achieved 70-80% confluency, the cells were trypsinized and seeded onto culture slides (BD Falcon, Bedford, MA) at a density of  $6.0 \times 10^5$  cells per well (surface area of 8  $\text{cm}^2$  per well) and incubated for 24 h at 37  $^{\circ}\text{C}$ . HCPT and Rb1/HCPT NPs ( $\text{IC}_{50}$ ) was added and incubated for 4 h at 37  $^{\circ}\text{C}$ . After incubation, all reagents were removed. Cells were washed with PBS (pH 7.4) at least 3 times and fixed with 4% formaldehyde solution for 10 min. The liquid content was then dried completely. The nuclei were then counterstained by DMEM medium with 4',6-diamidino-2-phenylindole (DAPI) (H-1200; Vector Laboratories, Inc., Burlingame, CA) for 15 min. The fixed cell monolayer was finally washed thrice by PBS and observed by CLSM (TCS SP5, Leica).

## 2.9. Pharmacokinetic experiments in mice

Tumor-free healthy C57BL/6 female mice were injected intravenously via the tail vein (six mice per group) with free BA, DHA, HCPT, Rb1/BA NPs, Rb1/DHA NPs and Rb1/HCPT NPs. After intravenous administration, 200  $\mu\text{L}$  blood samples were collected at 0.083, 0.25, 0.5, 1, 2, 5, 10, 24, 48, 72 h and centrifuged immediately at 3000 rpm for 10 min at 4  $^{\circ}\text{C}$ . To determine the concentration of total drugs in each plasma sample, 100  $\mu\text{L}$  of plasma was treated by 50  $\mu\text{L}$  of 0.1 N NaOH in water bath at 37  $^{\circ}\text{C}$  for 15 min, allowing the hydrolysis of the nanoparticles. After that, 0.1 N HCl (50  $\mu\text{L}$ ) was added, followed by 100  $\mu\text{L}$  methanol. After vortexed for 2 min, the mixture was sonicated for 5 min and centrifuged at 5000 rpm for 5 min. The clear supernatant was dried under nitrogen, reconstituted by 100  $\mu\text{L}$  methanol before HPLC analysis.<sup>32</sup> The HPLC employs a VYDAC 214TP54 (C18, 5 $\mu\text{m}$ , 4.6  $\times$  250 mm) with a UV detector (210 nm, 85:15 mixture (v/v) of acetonitrile-water as a mobile phase, flow rate at 1.0 mL/min). Blood circulation data were plotted as the blood BA, DHA, or HCPT levels with the unit of percentage of injected dose per gram (% ID/g) against time after injection.

## 2.10. In vivo efficacy studies

Subcutaneous tumor xenograft models were induced in the right axillary flank region of female C57BL/6 mice (6-7 weeks) after injection of  $3 \times 10^6$  LLC cells. Treatments were initiated when tumors reached an average volume of 100 to 150  $\text{mm}^3$ , and this day was designated as day 0. On day 0, these mice were randomly divided into 5 groups (n = 6) and administered intravenous injection with PBS (control), Rb1 NPs (20 mg/kg), free BA, DHA, and HCPT (10 mg/kg), Rb1/BA NPs, Rb1/DHA NPs and Rb1/HCPT NPs (10 mg BA, DHA, or HCPT-equivalent/kg), respectively, on days 0, 2, 4, 6, and 8. It is important to note that the concentrations of Rb1/BA NPs, Rb1/DHA NPs and Rb1/HCPT NPs stated in this article refer to free drug equivalents. For example, a dose of 10 mg/kg of Rb1/BA NPs means that the dose contains 10 mg/kg of BA and 28.45 mg/kg of whole nanoparticles, assuming that the loading of BA in the whole nanoparticles is 35.15%. In the observation phase, mice were monitored for tumor sizes and body weights every other day. Tumor volume was calculated using the formula:  $(L \times W^2)/2$ , where  $L$  is the longest and  $W$  is the shortest tumor diameter (millimeter).<sup>33, 34</sup> Relative tumor volume (RTV) was calculated at each measurement time point (where RTV was equal to the tumor volume at a given time point divided by the tumor volume prior to initial treatment). For efficacy studies, the percentage of tumor growth inhibition (%TGI) was calculated using the following formula:  $[(C - T)/C] \times 100$ , where  $C$  is the mean tumor volume of the control group at a specified time and  $T$  is the mean tumor volume of the treatment group at the same time. To monitor potential toxicity, we measured the weight of each mouse. At the end of the experiment (> 6 weeks) or the implanted tumor volume reached to 5000  $\text{mm}^3$ , the mice were sacrificed for humane reasons. To further evaluate the hematological toxicity of the nanoparticles, 200  $\mu\text{L}$  of blood was sampled from each mouse after final administration to test the white blood cell number (WBC) using a hematology analyzer (MEK-7222K, Nihon Kohden Celltac E).

## 2.11. Detection of allergic reaction

Toxic side-effects of the current chemotherapeutic drugs are often causing a severe reduction in the quality of life, so the detection of allergic reaction is very necessary and important. During the early development of drugs, type I hypersensitivity is the most common type of the hypersensitivity reaction. Some of the natural anti-cancer drugs, such as paclitaxel, docetaxel, and teniposide cyclosporine, were usually associated with a high incidence of the type I hypersensitivity reaction. It has been demonstrated that IgE antibodies play an important part in mediating type I hypersensitivity responses. We thus selected IgE levels as the parameter for rapid evaluation of type I hypersensitivity reactions. Five groups of tumor bearing mice (26-28 g, n = 6) were used in allergy testing studies (control, BA, DHA, HCPT, Rb1/BA NPs, Rb1/DHA NPs and Rb1/HCPT NPs). The samples were administered via tail intravenous injection every two days at the drug dose of 10 mg/kg body weight. After administration with different samples for 10 days, orbit blood of mice in different groups was collected and centrifuged. Serum samples were analyzed according to the procedure of mouse IgE ELISA.

## 2.12. Statistical analysis

All experiments in this study were performed at least three times, and the data were expressed as the means standard deviation (SD). Statistical analyses were performed by analysis of variance (ANOVA). In all analyses,  $p < 0.05$  was taken to indicate statistical significance.

## 3. Results and Discussion

### 3.1. Characterization of nanoparticles

A green natural drug delivery system Rb1 nanoparticle has been developed (Fig. 1A). The Rb1 readily forms nanoparticles in aqueous solutions.<sup>35</sup> We have encapsulated BA, DHA, and HCPT as the model chemotherapy drug into the Rb1 NPs for anticancer therapy. Hydrophobic drugs can be encapsulated into hydrophobic triterpene of Rb1 NPs, and the sugar side chains outer shell could improve the water-solubility and particle stability.<sup>36</sup> The mean drug loading capacity of Rb1/BA NPs, Rb1/DHA NPs, and Rb1/HCPT NPs was estimated to be  $35.15 \pm 2.76\%$ ,  $32.73 \pm 2.55\%$ , and  $21.36 \pm 2.18\%$  respectively. The TEM image of Rb1 NPs, Rb1/BA NPs, Rb1/DHA NPs and Rb1/HCPT NPs showed that the developed nanoparticles were spherical in shape with a low-level of agglomerations (Fig. 1B, C, D, and E). The smaller particles without black core might be the Rb1 NPs that contain no drugs.

Desired particles of Rb1/BA NPs, Rb1/DHA NPs and Rb1/HCPT NPs were produced provided the concentration of Rb1 and BA (DHA or HCPT) in the solvent solution ranged from 1 to 5 mg/mL and 0.5 to 4 mg/mL, respectively. It was observed that particles formed from 3 mg/mL Rb1 and 2 mg/mL BA (DHA or HCPT) were approximately 100 nm in size (Fig. 2A, B, and C,

**Table 1** Particle size, zeta potential and drug loading capacity of nanoparticles

Compound	size (nm)	zeta potential (mV)	DLC of drug (wt %)
Rb1 NPs	$67.3 \pm 10.2$	---	---
Rb1/BA NPs	$103.5 \pm 12.7$	$-14.8 \pm 0.5$	$35.15 \pm 2.76$
Rb1/DHA NPs	$99.8 \pm 11.8$	$-15.6 \pm 0.6$	$32.73 \pm 2.55$
Rb1/HCPT NPs	$131.2 \pm 15.6$	$-12.2 \pm 0.8$	$21.36 \pm 2.18$

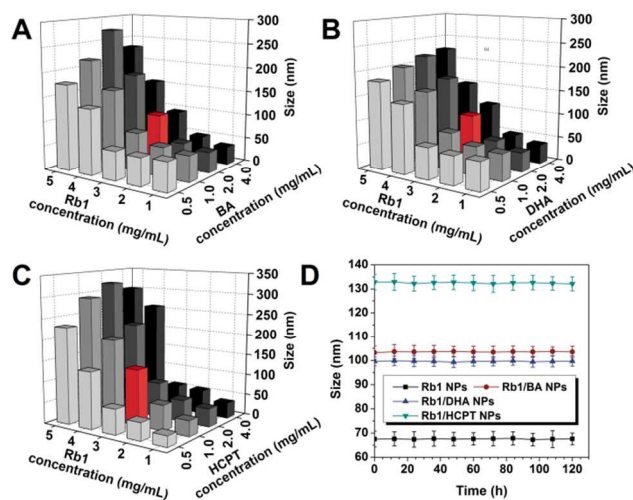


**Fig. 2** Size of Rb1/BA NPs (A), Rb1/DHA NPs (B), and Rb1/HCPT NPs (C) formed with different concentrations of Rb1, and free drugs. (D) The size distribution of the nanoparticles for 120 hours of storage at 4 °C.

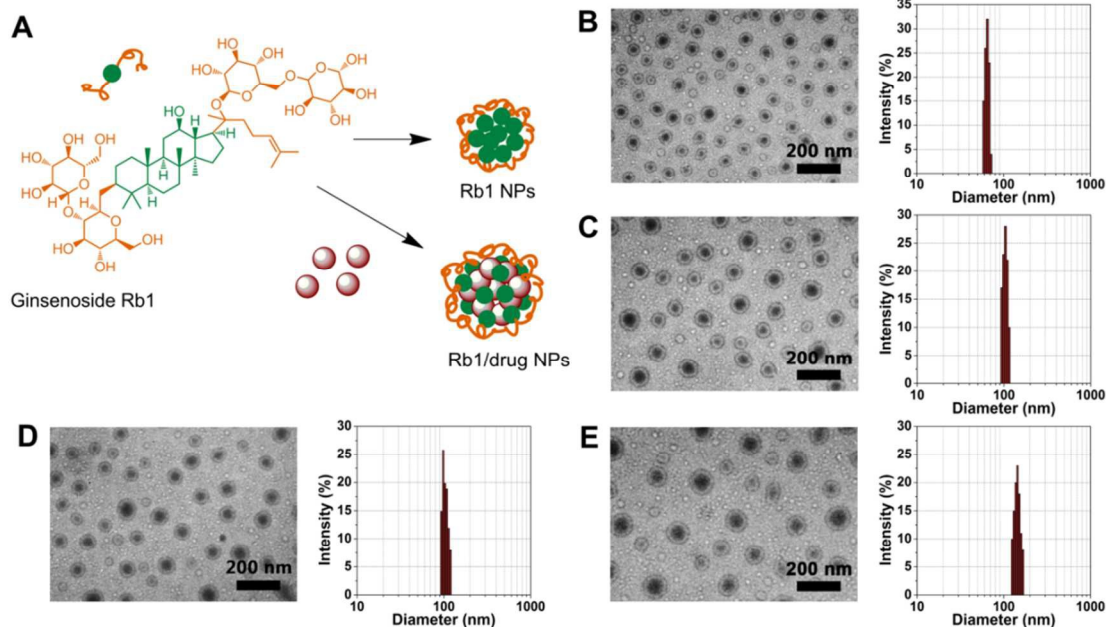


**Fig. 1** Schematic diagram and morphology of self-assembled Rb1 NPs loaded with anticancer drugs. (A) Schematic of the self-assembly process used to form the Rb1 NPs, which are formed via self-assemblies in an aqueous solution: BA, DHA, or HCPT was encapsulated into hydrophobic triterpene of Rb1 NPs, and the sugar side chains outer shell could improve the water-solubility and particle stability. TEM images and hydrodynamic size distributions of Rb1 NPs (B), Rb1/BA NPs (C), Rb1/DHA NPs (D), and Rb1/HCPT NPs (E) were observed, respectively.

Cite this: DOI: 10.1039/c0xx00000x

www.rsc.org/xxxxxx

PAPER

Table 1). However, when the free drug concentration was increased while keeping the Rb1 concentration constant, the nanoparticle size increased up to a maximum, followed by a decrease with a further increase in free drug concentration. The approximately 100 nm nanoparticle system suggested its potential for effective tumor targeting *in vivo*.<sup>37</sup> In addition, as shown in Fig. 2D, the average particle size of the nanoparticles (redispersion in PBS) hardly changed during the investigation period, i.e. the nanoparticles exhibited good redispersion stability.

The zeta potential is a key factor to consider when evaluating the stability of a colloidal dispersion. The internalization of negatively charged nanoparticles is believed to occur through nonspecific binding and clustering of the particles on cationic sites on the plasma membrane (that are relatively scarcer than negatively charged domains) and their subsequent endocytosis. Rb1/BA NPs, Rb1/DHA NPs and Rb1/HCPT NPs all have a negative surface charge ( $\xi = 14.8$  Mv, 15.6 mV, and 12.2 mV). The interparticle interactions may be partly responsible for the charge of the nanoparticles to easily disperse, which enables Rb1/BA NPs, Rb1/DHA NPs and Rb1/HCPT NPs to be easily resuspended after a period of sedimentation.<sup>38</sup>

It was reported that ginsenoside Rb1 can form the nanoparticle above the critical aggregation concentration (CAC) of 339  $\mu\text{g}/\text{mL}$  in de-ionized water.<sup>39</sup> As Rb1/BA NPs were stable at the CAC, it is probable that these particles will remain stable at high dilution in biological systems. For example, in a 27 g mouse model treated at 10 mg/kg BA, 200  $\mu\text{L}$  of Rb1/BA NPs administered *i.v.* (390  $\mu\text{g}/\text{mL}$  Rb1/BA NPs) would be diluted in  $\sim 2$  mL blood volume to 390  $\mu\text{g}/\text{mL}$  Rb1/BA NPs. Considering the scenario when 90% of particles are out of circulation, the concentration of Rb1/BA NPs would be still well above CAC.

### 3.2. *In vitro* drug release

Nanoparticles with suitable size were first placed in aqueous solutions that simulated biological fluids. The resulting release data appear in Fig. 3 suggested that BA, DHA, and HCPT encapsulated with nanoparticles revealed a slightly initial burst (more than 20%, at 0–6 hours). The slightly initial burst release of drugs from the nanoparticles was credited to lipophilic molecules located within the shell or at the core and shell

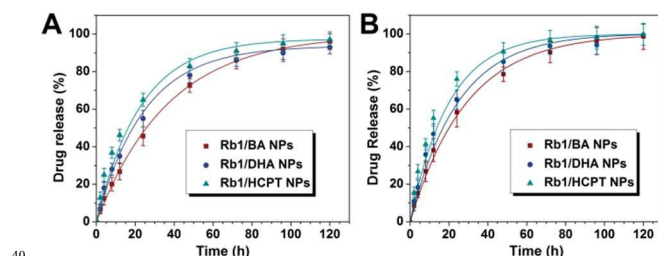


Fig. 3 BA, DHA, and HCPT release kinetics in buffer at pH 7.4 (A) and pH 4.5 (B) and 37 °C from the nanoparticles, respectively.

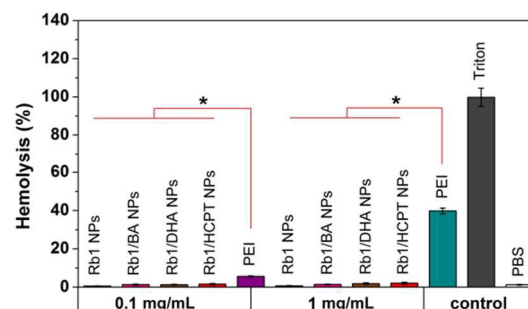


Fig. 4 *In vitro* hemolysis assay of Rb1 NPs, drug loading nanoparticles compared to PEI<sub>25K</sub> and Triton X-100 measured at 541 nm. Values are reported as the mean  $\pm$  SD for triplicate samples.

interface of the nanoparticles. Furthermore, an initial burst in release may be attributed to balancing the equilibrium between the inside and outside release settings. Rb1/BA NPs showed the slower release from the nanoparticles which could be attributed to a more effective drug/carrier interaction for Rb1/BA mixed nanoparticles. Rb1 and BA are all the polycyclic triterpenoids. In addition to hydrophobic interaction of Rb1 with BA, the  $\pi$ - $\pi$  stacking also contribute to the overall carrier/BA interaction.<sup>40</sup> The resulting release data appear in Fig. 3. The amount of drug loading as listed in Table 1.

### 3.3. Hemolysis study

Detrimental interaction of nanoparticles with blood constituents such as RBCs must be avoided when these nanoparticles are injected into the blood circulation as a carrier for drug delivery.<sup>28</sup> Erythrocytes were incubated with two concentrations of samples as 1 mg/mL and 0.1 mg/mL, for 1 h at 37 °C. Hemolysis was evaluated by measuring the amount of hemoglobin released in the supernatant at 541 nm (Fig. 4). Triton X-100 as positive control, which induced full hemoglobin release. Nanoparticles at concentrations of 1 mg/mL and 0.1 mg/mL showed a comparable hemoglobin release to blank values (<5%), which was significantly lower than similar concentrations of PEI<sub>25K</sub>, a cationic polymer known to have significant hemolytic effect. Despite BA, DHA, and HCPT was cytotoxic to the RBCs in a previous study,<sup>41, 42</sup> Drug loading nanoparticles have been released little drugs during the short incubation period. In this study, the nanoparticles did not cause any, or only mild, adverse reactions. This may be due to the anti-hemolytic properties of the ginsenoside Rb1.<sup>43</sup>

### 3.4. *In vitro* cytotoxicity

To ensure the effective of the drug delivery before their entry into human application, *in vitro* cytotoxicity should be considered upfront. The cytotoxicity of free BA, DHA, HCPT, Rb1 NPs, and drug-loading nanoparticles to LLC cancer cells was evaluated using the CCK-8 assay. Analysis of *in vitro* cytotoxicity

measurements showed that free drugs (10  $\mu\text{g}/\text{mL}$ ) induced cell death which was dependent upon length of incubation. As shown in Fig. 5A, the time-dependent cytotoxic effect of the Rb1/BA NPs, Rb1/DHA NPs and Rb1/HCPT NPs was evident, which indicated that 33.9 %, 32.7%, and 29.8 survival after 24 h, 23.8 %, 21.8%, and 20.1 survival after 48 h and 13.9 %, 12.1%, and 10.0% survival after 72 h at 10  $\mu\text{g}/\text{mL}$  (equivalent to native drugs). The drug release from the nanoparticles when incubated with cells, is possibly from the diffusion of drug molecules in the nanoparticles, which is the main mechanism of drug release observed for polymer nanoparticles.<sup>44</sup>

To compare the potency of the nanoparticles, the concentrations of drug which killed 50% of the cells ( $\text{IC}_{50}$ ) were estimated from survival curves as shown in Fig. 5B, C, and Table 2, obtained from replicate experiments. The results showed that the  $\text{IC}_{50}$  of the sample is in the order BA > Rb1+BA > Rb1/BA NPs > DHA > Rb1+DHA > Rb1/DHA NPs > HCPT > Rb1+HCPT > Rb1/HCPT NPs (Table 2). It is hard not to read messages into the results of adding Rb1 and free drugs directly, the combination therapy with Rb1 can induce superior *in vitro* therapeutic efficacy versus free drugs. Moreover, compared to free drug groups, Rb1/BA NPs, Rb1/DHA NPs, and Rb1/HCPT NPs treatment was 1.5 $\times$ , 1.7 $\times$  and 1.7 $\times$  more toxic against LLC, respectively. Increased drug-loading nanoparticles toxicity was approximately related to the chemosensitivity of each cell line and slow release of the drugs.

### 3.5. The pharmacokinetics in mice

Long blood circulation half-time of a drug carrier is desired to improve the bioavailability of the drug. For most nanomedicine, this has been a worthwhile goal. Here, the pharmacokinetics of nanoparticles was studied after i.v. administration to C57BL/6

**Table 2** *In vitro* cytotoxicity analysis ( $\text{IC}_{50}$ ,  $\mu\text{g}/\text{mL}$ )

Compound	LLC
Rb1 NPs	---
BA	6.35 (0.51935)
Rb1+BA	5.88 (0.50261)
Rb1/BA NPs	4.17 (0.38536)
DHA	0.83 (0.02235)
Rb1+DHA	0.69 (0.01952)
Rb1/DHA NPs	0.50 (0.02302)
HCPT	0.31 (0.02936)
Rb1+HCPT	0.29 (0.02108)
Rb1/HCPT NPs	0.18 (0.01563)

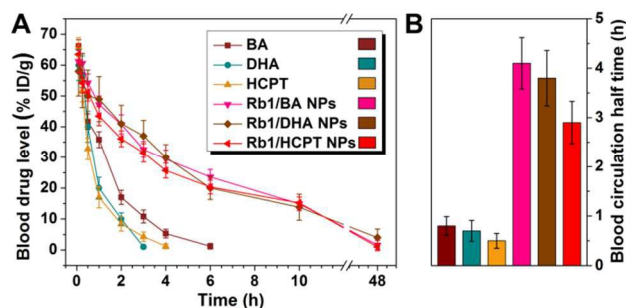


**Fig. 6** Blood circulation data in C57BL/6 mice. (A) Blood circulation curves of different groups. Error bars were based on six mice per group at each time point. (B) Blood circulation half-time of different groups obtained.

mice. The determined drug concentration after hydrolysis under basic condition was actually the total drugs in plasma, the combination of both parent form and nanoparticles form. The blood clearance profiles of free drugs and nanoparticles in mice were shown in Fig. 6A and B. Disappearance of free BA, DHA, and HCPT from the blood circulation after intravenous

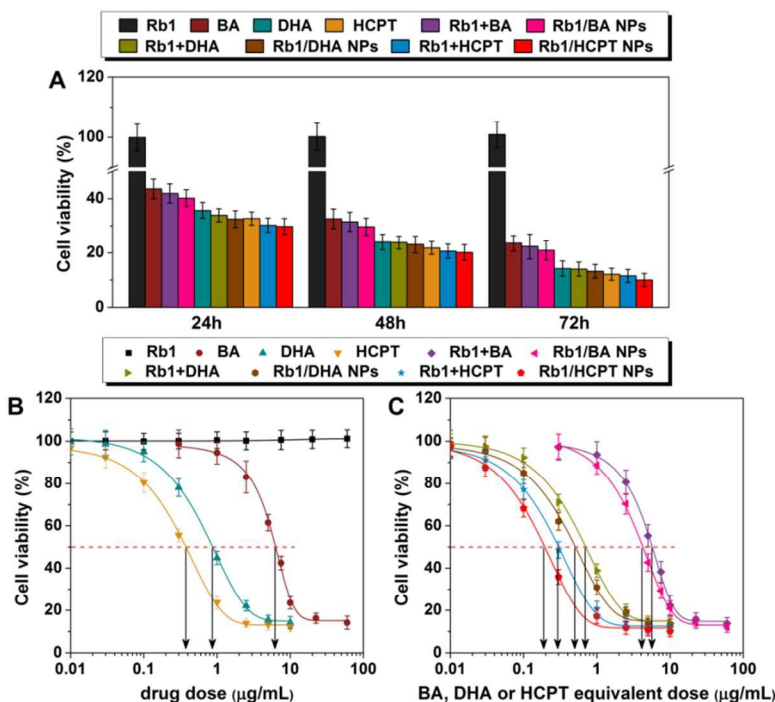


**Fig. 5** (A) Cell viability of LLC cells treated with 10  $\mu\text{g}/\text{mL}$  of different drugs or drug formulations (equivalent to native drugs) was measured by CCK-8 assay ( $n=3$ , error bars represent standard deviation). (B) CCK-8 assay of all groups with different concentrations in LLC cell lines ( $n=3$ , error bars represent standard deviation).

Cite this: DOI: 10.1039/c0xx00000x

www.rsc.org/xxxxxx

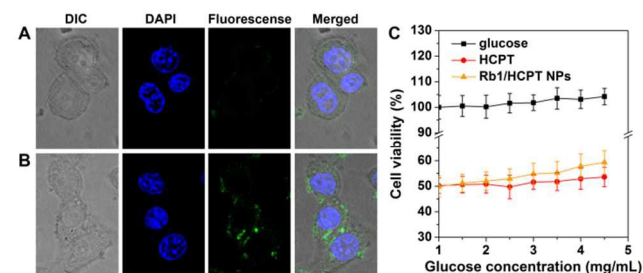


**Fig. 7** Confocal microscopic pictures of LLC cells incubated with (A) free HCPT and (B) Rb1/HCPT NPs at an equivalent HCPT concentration ( $IC_{50}$ ) for 4 h at 37 °C. (C) Effect of glucose on viability of LLC incubated with Rb1/HCPT NPs.

administration of injection was very rapid with the plasma concentration below 10% of injected dose per gram (% ID/g) at 3 h, 2 h, and 2 h, respectively. On the contrary, Rb1/BA NPs, Rb1/DHA NPs and Rb1/HCPT NPs exhibited a remarkable prolonged clearance with the free drug levels of 15.2%, 14.7% and 15.8% ID/g, respectively, at 10 h after administration. Rb1/BA NPs, Rb1/DHA NPs and Rb1/HCPT NPs could extend the blood circulation half-time of BA, DHA, and HCPT from 0.8 h to 4.1 h (5.1- fold), 0.7 h to 3.8 h (5.4- fold) and 0.5 h to 2.9 h the blood circulation half-time of BA, DHA, and HCPT from 0.8 h to 4.1 h (5.1- fold), 0.7 h to 3.8 h (5.4- fold) and 0.5 h to 2.9 h (5.8- fold), respectively, which were far longer than values of free drugs. The slow release and particle size of the nanoparticles was important for obtaining long circulation.

### 3.6. Cellular uptake

As shown in Fig. 7, the cellular uptake efficiencies of HCPT and Rb1/HCPT NPs were evaluated by CLSM. It can be visualized the fluorescence of HCPT (green) and the DAPI (blue). Free HCPT molecules transported into the cytoplasm of the cell, in a passive diffusion manner, were effluxed out by P-glycoprotein pumps, while some of them could reach into the nucleus and bind to DNA. In general, HCPT-loaded nano-particulates, such as liposomes, micelles, polymer nanoparticles, have been known to be taken up by cells through an endocytic pathway, thereby making them escape from the effect of P-glycoprotein pumps. The endocytic delivery of HCPT within cells by using nanoparticles maintains the intracellular HCPT concentration to be high in the cytoplasm region. This can be seen in Fig. 7A and B. Cellular uptake extent of Rb1/HCPT NPs was significantly higher than free HCPT under the same condition.

Moreover, tumors have a special metabolism. Among the many differences with non-transformed tissues, perhaps the most relevant is that they rely on glucose as a source of energy and carbon. Tumors seek glucose so avidly, for this reason, glucose analogs could be used for targeted drug delivery in pharmaceutical applications.<sup>25</sup> Certain sugar modifications have

**Table 3** LLC xenograft model (q2d × 5): efficacy comparison

Compound	mean TV±SD <sup>a</sup> (mm <sup>3</sup> )	RTV <sup>a</sup>	TGI <sup>a</sup> (%)	Cures <sup>b</sup> (%)
control	5016 ± 2059	38.0 ± 15.6	0	0
BA	2553 ± 1490	18.5 ± 10.8	44.0	0
DHA	2482 ± 1222	19.6 ± 9.5	45.6	0
HCPT	2849 ± 1480	20.8 ± 10.7	37.5	16.7
Rb1/BA NPs	1258 ± 460	10.4 ± 3.8	72.4	33.3
Rb1/DHA NPs	1225 ± 512	9.8 ± 4.1	73.1	33.3
Rb1/HCPT NPs	1310 ± 668	10.0 ± 5.1	71.3	33.3

<sup>a</sup> Mean tumor volume (TV), RTV, and % TGI data were taken at day 20. (By day 20, a significant percentage of control animals were euthanized due to excess tumor burden.) <sup>b</sup> % cures were taken at day 26.

been associated with reduced affinity for P-glycoprotein pumps and maintenance of cytotoxic activity. In order to further evaluate the role of the sugar side chains in the cellular uptake of nanoparticles, the LLC cells were incubated with the nanoparticles ( $IC_{50}$ ) in culture medium containing increasing concentrations of glucose. The cytotoxicity of Rb1/HCPT NPs against LLC cells was inhibited by excess free folate, and the cell viability increased with increasing glucose concentration. However, HCPT cytotoxicity did not change as a function of folate concentration (Fig. 7B). For instance, the cell viability of Rb1/HCPT NPs against LLC cells was approximately 15.2% at glucose concentrations of 1.0 mg/mL, but it was about 40% in the presence of 4.5 mg/mL glucose. These findings suggest that glucose prevent the cellular uptake of the nanoparticles with the sugar side chains.

### 3.7. In vivo studies

The results obtained above gave us a lot of motivated to explore the antitumor efficacy of the nanoparticles in a mouse tumor model. *In vivo* antitumor efficiency of drug delivery nanoparticles were compared with free drugs at equivalent doses (10 mg/kg) on multiple-dose schedule in xenograft models of lung tumor. For humane reasons, animals were killed and regarded as dead if the implanted tumor volume reached 5000 mm<sup>3</sup> or at the end of the experiment (> 6 weeks). Tumor-bearing mice treated with the nanoparticles showed a clear survival advantage compared with the control treated mice (Fig. 8B). As shown in Fig. 8A, the groups treated with BA, DHA, HCPT, and nanoparticles showed varied levels of antitumor effects. The treatment with Rb1/BA NPs, Rb1/DHA NPs, and Rb1/HCPT NPs resulted in 72.4%, 72.4% , and 71.3% TGI (day 20), respectively, and 33.3% survival of animals (day 30). In contrast, multiple-dose free drug treatment resulted in 44.0%, 45.6%, and 37.5% TGI (day 20), respectively, and survival rate was zero (day 30) (Fig. 8A and B, Table 3). Importantly, in line with the literature, no signs of systemic toxicity were observed by monitoring general behavior, appetite and mice body weight (Fig. 8C).

As expected, when using the free drugs encapsulated Rb1 NPs

Cite this: DOI: 10.1039/c0xx00000x

PAPER

www.rsc.org/xxxxxx

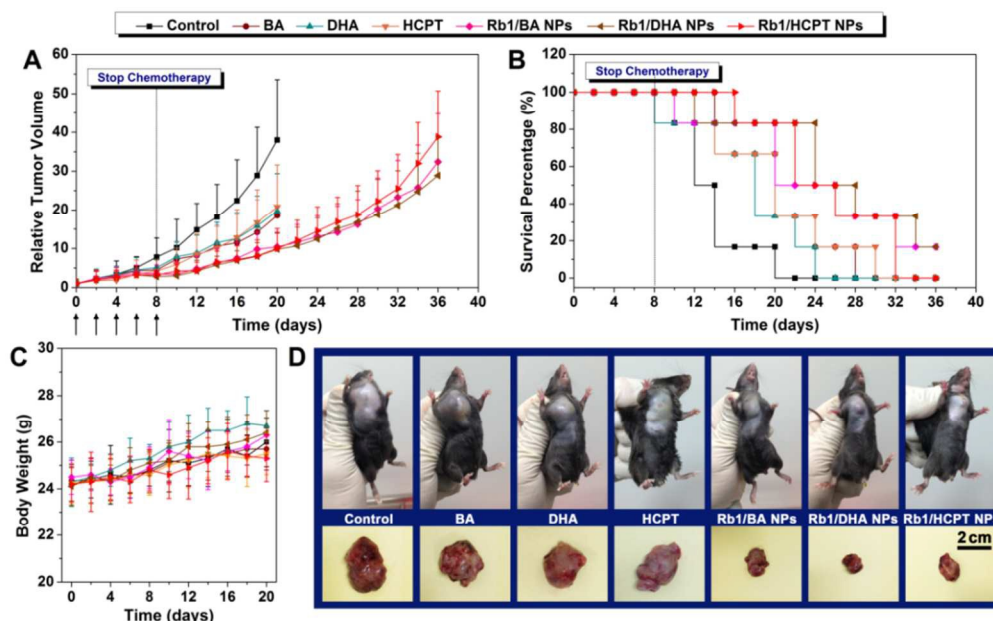


Fig. 8 Antitumor efficacy of free drugs and drug loading nanoparticles in the subcutaneous mouse model of LLC. (A) Relative tumor volumes of mice during treatment with different groups. (B) Survival of mice in different treatment. (C) Tumor photographs from each treatment group excised on day 20.

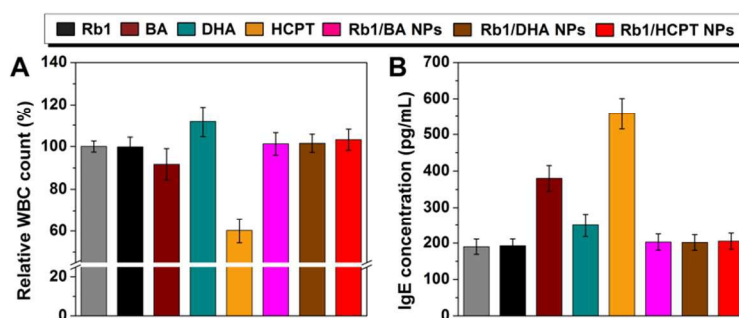


Fig. 9 (A) White blood cell (WBC) change during four administrations in normal mice with free drugs and nanoparticles. Blood sample was collected from mice on day 2 after the last dosage treatment. (B) IgE levels of mice treated with different groups for 30 min. Data as means  $\pm$  SD; n = 6.

for *in vivo* anti-tumor therapy, three effects are anticipated to increase the uptake of the drug-loaded nanoparticles by cancerous cells: (1) the appropriate size ( $\sim 100$  nm), the EPR effect of solid tumors would allow more drug-loaded nanoparticles to be accumulated in the tumor tissue;<sup>45</sup> (2) high drug loading ( $\sim 35$  wt% BA,  $\sim 33$  wt% DHA, and  $\sim 21$  wt% HCPT); (3) drug-loaded nanoparticles can increase the solubility of the drug.<sup>46</sup> In addition, the *in vitro* and *in vivo* experiments demonstrate that the Rb1 may have the functions of increasing efficacy of the free anticancer drugs. The Rb1 shell of the nanoparticles could decrease the harmful side effects.

### 3.7. Evaluation of the side effects

During the early development of new drug, many drug

formulations, such as paclitaxel, docetaxel, and teniposide cyclosporine are always associated with serious side effects including hematological toxicity and hypersensitivity reactions (usually type I hypersensitivity). Therefore, we tested the potential side effects of nanoparticles. To examine the type I hypersensitivity responses, the IgE antibody level, the parameter for rapid evaluation, was detected in each group. The blood IgE levels of mice in different groups were shown in Fig. 9A. Mice treated with free drugs displayed a higher IgE level than the control group, which might be ascribed to the bad water solubility. As expected, no significant change of IgE level was observed in the nanoparticle groups, which explored the idea that the use of these nanoparticles could reduce the risk of hypersensitivity reactions substantially. The blood of mice after treatment with

Cite this: DOI: 10.1039/c0xx00000x

www.rsc.org/xxxxxx

different formulations was also collected to test the WBC count, which is often used as an indicator of hematologic toxicity. The total WBC count of mice treated with BA and HCPT showed a little decrease the normal group (Fig. 9B). The significant increase of WBC count is an indication of the immune boosting capacity of the DHA in rats. No discernible decreases in WBC number of the mice treated with nanoparticles were observed, indicating that the nanoparticles designed in this study could avoid severe hematotoxicity.

#### 4. Conclusion

Green preparation of medicated nanoparticles emerges as an attractive discipline to produce the pharmaceutical formulations. Green nanoparticles loaded with drugs reduce the use of toxic and harmful ingredients in the production process and provide the lower-dose prescribing for medical treatments. In this study, we have developed and characterized a ginsenoside-based nanoparticle for anticancer drug delivery where the carrier itself displays health efficacy. This system was formulated by the simple self-assembly of ginsenoside Rb1 and anticancer drugs (BA, DHA, or HCPT), which avoided the human and environmental risks caused by the potential toxicity of the chemosynthetic excipients. This ginsenoside Rb1 nanoparticle for delivery of anticancer drugs demonstrated a series of attractive properties as an anticancer drug delivery carrier, including ease of preparation, appropriate size, better tumor selectivity, high loading capacity of drugs, good stability, and no side effects. We suggest that the green ginsenoside Rb1 nanoparticles could be an efficient general method in various indissolvable drug deliveries.

#### Acknowledgements

This study was funded by the State Forestry Administration 948 Project of China (No. 2014-4-35), the Fundamental Research Funds for the Central Universities (200-1244951), Beijing Natural Science Foundation of China (Grant No. 2142024), and the National Natural Science Foundation of China (No. 21576029).

#### Notes and references

<sup>a</sup> Beijing Key Laboratory of Lignocellulosic Chemistry, Beijing Forestry University, Beijing 100083, P. R. China. Fax/Tel: 8610-62337251; E-mail: ljd2012@bjfu.edu.cn

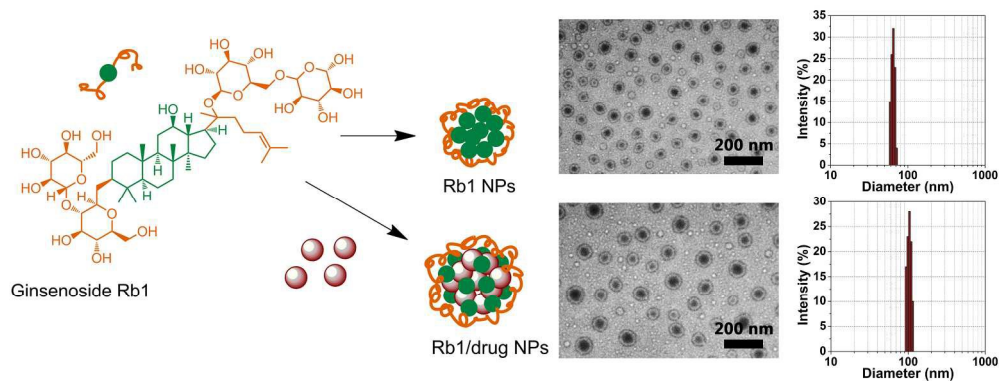
<sup>b</sup> Tianjin Key Laboratory of Pulp & Paper, College of Materials Science & Chemical Engineering, Tianjin University of Science & Technology, Tianjin 300457, P. R. China

1. T. M. Allen and P. R. Cullis, *Science*, 2004, **303**, 1818-1822.
2. J. Clark, R. Sheldon, C. Raston, M. Poliakoff and W. Leitner, *Green Chemistry*, 2014, **16**, 18-23.
3. L. Vaccaro, D. Lanari, A. Marrocchi and G. Strappaveccia, *Green Chemistry*, 2014, **16**, 3680-3704.

4. L. Dai, L. Wang, L. Deng, J. Liu, J. Lei, D. Li and J. He, *Scientific Reports*, 2014, **4**, 5871.
5. L. Dai, L.-Y. Wang, T.-Q. Yuan and J. He, *Polymer Degradation and Stability*, 2014, **99**, 233-239.
6. L. Dai, T. Yang, J. He, L. Deng, J. Liu, L. Wang, J. Lei and L. Wang, *Journal of Materials Chemistry B*, 2014, **2**, 6749-6757.
7. L. Dai, K.-F. Liu, C.-L. Si, J. He, J.-D. Lei and L.-Q. Guo, *Journal of Materials Chemistry B*, 2015, **3**, 6605-6617.
8. L. Xu, H. Yu, S. Yin, R. Zhang, Y. Zhou and J. Li, *J Nanopart Res*, 2015, **17**, 1-13.
9. T.-H. Kim and S.-M. Lee, *Food and Chemical Toxicology*, 2010, **48**, 1516-1520.
10. D. Zhu, L. Wu, C.-R. Li, X.-W. Wang, Y.-J. Ma, Z.-y. Zhong, H.-B. Zhao, J. Cui, S.-F. Xun, X.-L. Huang, Z. Zhou and S.-Q. Wang, *Journal of Cellular Biochemistry*, 2009, **108**, 117-124.
11. Q.-Y. Li, L. Chen, W.-H. Fu, Z.-D. Li, B. Wang, X.-J. Shi and M.-K. Zhong, *Journal of agricultural and food chemistry*, 2011, **59**, 6312-6318.
12. W. Chen, Y. Guo, W. Yang, P. Zheng, J. Zeng and W. Tong, *Exp Brain Res*, 2015, **233**, 2823-2831.
13. S. Zhang, J. Deng, Y. Gao, D.-l. Yang, Q.-h. Gong and X.-n. Huang, *European Journal of Pharmacology*, 2012, **685**, 126-132.
14. A.-W. Shi, N. Gu, X.-M. Liu, X. Wang and Y.-Z. Peng, *Journal of International Medical Research*, 2011, **39**, 1306-1318.
15. M. R. Harkey, G. L. Henderson, M. E. Gershwin, J. S. Stern and R. M. Hackman, *The American Journal of Clinical Nutrition*, 2001, **73**, 1101-1106.
16. S. Sengupta, S.-A. Toh, L. A. Sellers, J. N. Skepper, P. Koolwijk, H. W. Leung, H.-W. Yeung, R. N. S. Wong, R. Sasisekharan and T.-P. D. Fan, *Circulation*, 2004, **110**, 1219-1225.
17. S. Gao, S. Basu, Z. Yang, A. Deb and M. Hu, *Current Drug Targets*, 2012, **13**, 1885-1899.
18. J. Zhao, C.-h. Yang, M. Hu and Z.-q. Liu, *Nan Fang Yi Ke Da Xue Xue Bao*, 2009, **29**, 2387-2390.
19. S. Mitra and S. R. Dungan, *Journal of agricultural and food chemistry*, 1997, **45**, 1587-1595.
20. S. Mitra and S. R. Dungan, *Journal of agricultural and food chemistry*, 2001, **49**, 384-394.
21. O. Güçlü-Ustündağ and G. Mazza, *Crit Rev Food Sci Nutr*, 2007, **47**, 231-258.
22. Y. Tu, C. Yang, Y. Cheng, G. Zeng, L. Lu and L. Wang, *Bioresource Technology*, 2015, **175**, 231-238.
23. X. Dai, X. Shi, Q. Yin, H. Ding and Y. Qiao, *Journal of Colloid and Interface Science*, 2013, **396**, 165-172.
24. S. C. Owen, D. P. Y. Chan and M. S. Shoichet, *Nano Today*, 2012, **7**, 53-65.
25. N. El Mjijad, A. Caro-Maldonado, S. Ramirez-Peinado and C. Munoz-Pinedo, *Oncogene*, 2011, **30**, 253-264.
26. J. Ge, E. Neofytou, J. Lei, R. E. Beygui and R. N. Zare, *Small*, 2012, **8**, 3573-3578.
27. H.-Y. Cheung and Q.-F. Zhang, *Journal of Chromatography A*, 2008, **1213**, 231-238.
28. R. Reul, J. Nguyen and T. Kissel, *Biomaterials*, 2009, **30**, 5815-5824.
29. J. Nguyen, T. W. J. Steele, O. Merkel, R. Reul and T. Kissel, *Journal of Controlled Release*, 2008, **132**, 243-251.
30. W. Wei, P. P. Lv, X. M. Chen, Z. G. Yue, Q. Fu, S. Y. Liu, H. Yue and G. H. Ma, *Biomaterials*, 2013, **34**, 3912-3923.
31. F. Unger, M. Wittmar and T. Kissel, *Biomaterials*, 2007, **28**, 1610-1619.

32. B. Shi, C. Fang and Y. Pei, *Journal of pharmaceutical sciences*, 2006, **95**, 1873-1887.
33. K. Kim, J. H. Kim, H. Park, Y. S. Kim, K. Park, H. Nam, S. Lee, J. H. Park, R. W. Park, I. S. Kim, K. Choi, S. Y. Kim, K. Park and I. C. Kwon, *Journal of controlled release : official journal of the Controlled Release Society*, 2010, **146**, 219-227.
34. M. J. Ernsting, M. Murakami, E. Undzys, A. Aman, B. Press and S. D. Li, *Journal of controlled release : official journal of the Controlled Release Society*, 2012, **162**, 575-581.
35. K. Koga, S. Kawashima, N. Shibata, K. Takada and M. Murakami, *Biological and Pharmaceutical Bulletin*, 2003, **26**, 1299-1305.
36. Y. Sanada, I. Akiba, K. Sakurai, K. Shiraiishi, M. Yokoyama, E. Mylonas, N. Ohta, N. Yagi, Y. Shinohara and Y. Amemiya, *Journal of the American Chemical Society*, 2013, **135**, 2574-2582.
37. Y. Huang, J. Lu, X. Gao, J. Li, W. Zhao, M. Sun, D. B. Stolz, R. Venkataramanan, L. C. Rohan and S. Li, *Bioconjugate chemistry*, 2012, **23**, 1443-1451.
38. H. L. Ma, Y. F. Xu, X. R. Qi, Y. Maitani and T. Nagai, *International Journal of Pharmaceutics*, 2008, **354**, 217-226.
39. T. Yamanaka, J.-P. Vincken, P. de Waard, M. Sanders, N. Takada and H. Gruppen, *Journal of agricultural and food chemistry*, 2008, **56**, 11432-11440.
40. X. Zhang, J. Lu, Y. Huang, W. Zhao, Y. Chen, J. Li, X. Gao, R. Venkataramanan, M. Sun, D. B. Stolz, L. Zhang and S. Li, *Bioconjugate chemistry*, 2013, **24**, 464-472.
41. M. Gao, P. M. Lau and S. K. Kong, *Archives of toxicology*, 2014, **88**, 755-768.
42. L. Fang, M. Wang, S. Gou, X. Liu, H. Zhang and F. Cao, *Journal of Medicinal Chemistry*, 2014, **57**, 1116-1120.
43. S. Hu, C. Concha, F. Lin and K. Persson Waller, *Veterinary Immunology and Immunopathology*, 2003, **91**, 29-37.
44. S. Fredenberg, M. Wahlgren, M. Reslow and A. Axelsson, *International Journal of Pharmaceutics*, 2011, **415**, 34-52.
45. H. Maeda, *Journal of Controlled Release*, 2012, **164**, 138-144.
46. O. P. Medina, N. Pillarsetty, A. Glekas, B. Punzalan, V. Longo, M. Gönen, P. Zanzonico, P. Smith-Jones and S. M. Larson, *Journal of Controlled Release*, 2011, **149**, 292-298.

40



245x94mm (300 x 300 DPI)